# Effective modelling of the Rayleigh-Bénard convection of concentrated emulsions with finite-size droplets

Francesca Pelusi,* Mauro Sbragaglia, and Roberto Benzi
*Department of Physics, University of Rome "Tor Vergata" & INFN - Via della Ricerca Scientifica 1, 00133 Rome, Italy*

Andrea Scagliarini and Massimo Bernaschi
*Istituto per le Applicazioni del Calcolo, CNR - Via dei Taurini 19, 00185 Rome, Italy*

Sauro Succi
*Istituto per le Applicazioni del Calcolo, CNR - Via dei Taurini 19, 00185 Rome & Center for Life Nano Science Sapienza, Istituto Italiano di Tecnologia - Viale Regina Elena 295, I-00161 Rome, Italy*



We present mesoscale numerical simulations of Rayleigh-Bénard convection in a two-dimensional concentrated emulsion, confined between two parallel walls, heated from below and cooled from above, under the effect of buoyancy forces. The systems under study comprise finite-size droplets, whose concentration $\Phi_0$ is varied, ranging from the dilute limit up to the point where the emulsion starts to be packed and exhibits non-Newtonian rheology. We focus on the characterisation of the convective heat transfer properties close to the transition from conductive to convective states. The convective flow is confined and heterogeneous, which causes the emulsion to exhibit concentration heterogeneities in space $\phi_0(y)$, depending on the location in the wall-to-wall direction ($y$). With the aim of assessing quantitatively the heat transfer efficiency of such heterogeneous systems, we resort to a side-by-side comparison between the concentrated emulsion system and a single-phase (SP) system, whose local viscosity $\eta^{\rm SP}(y)$ is suitably constructed from the shear rheology of the emulsion. Such comparison highlights that a suitable degree $\Lambda$ of coarse-graining needs to be introduced in the local viscosity $\eta^{\rm SP}_\Lambda(y)$, in order for the single-phase system to attain the same heat transfer efficiency of the emulsion. Specifically, it is shown that a quantitative matching between the two systems is possible whenever the coarse-graining is performed over a scale of the order of the droplet size.

## I. INTRODUCTION

Heat transfer in heterogeneous media made of dispersions of one phase (solid, liquid or gaseous) in another liquid phase is of paramount importance for an ample variety of technological applications [1, 2]. Depending on the dispersed phase, different types of systems can be obtained: dispersions of gas bubbles in a continuous liquid phase [3–7], dispersions of droplets in a liquid matrix [8–12], suspensions of particles dispersed in a liquid solvent [13–15]. The focus of this paper is on the characterisation of the heat transfer properties in a biphasic medium, consisting of deformable droplets of a liquid phase dispersed in another phase with the same viscosity. The mechanical response of these kind of systems has been thoroughly addressed in theory [16–22], simulations [23–26] and experiments [27–30], resulting in a very detailed characterisation of the response of the medium under flow when the concentration $\Phi_0$ of the dispersed phase changes systematically (see also [31–35] and references therein). One may refer, for example, to the vast knowledge on the deformation and break-up properties of single constituents (i.e. an emulsion in the extremely dilute limit) and/or the characterisation of the medium effective viscosity from dilute to semi-dilute concentrations [10, 36–39]. Such a very detailed knowledge is somehow not mirrored in a corresponding characterisation of the heat transfer properties of the medium. Few studies considered effective fluids with non-Newtonian constitutive laws for the stress tensor, focusing on the role of yield stress rheology [40–51]. Such models share, thus, some similarities with emulsions, even though the continuum nature of the approach inevitably overlooks finite droplet size effects. Actually, we may expect that, especially in confined systems and/or in concentrated dispersions, the *granularity* of the system will lead to a failure of any attempt of modelling by means of continuum equations or with point-like particles. With the present paper, we aim at addressing that issue via numerical simulations in the paradigmatic set-up of the Rayleigh-Bénard convection [52–57], i.e. when the emulsion is confined between two parallel plates heated from below and cooled from above, under a gravity field. We observe that, due to the convective dynamics, the emulsion develops a non-homogeneous droplet distribution across the cell. We then inspect the heat flux and compare the heterogeneous two-phase system with a single-phase (SP) fluid model with space-dependent effective viscosity, suitably constructed from the shear rheology of the emulsion. It is shown that, in order to get a quantitative matching between the two cases, a spatial averaging procedure ("coarse-graining") over a scale of the order of the droplet size is needed, thus identifying the origin of the effect within the *discrete* nature of these complex fluids.

The paper is organised as follows: in Section II we provide a brief overview of the methodology used; in Section III we report the results of the numerical simulations; conclusions follow in Section IV.

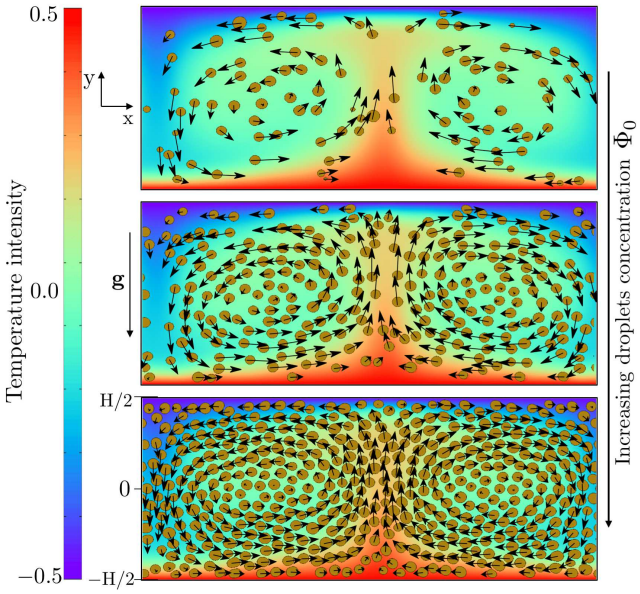


FIG. 1. Numerical simulations set-up: we study the Rayleigh-Bénard convection in two-dimensional concentrated emulsions made of droplets (dispersed phase, dark-yellow domains) into a continuous phase. The emulsions are placed between two parallel plates at fixed temperatures in $y = \pm H/2$, while gravity forces (buoyancy) act along the wall-to-wall direction. We focus on the convective regimes just above the transition from conduction to convection, where the systems display a temperature plume with a two-rolls structure in the velocity field (black arrows represent droplets displacements during convection). We focus on the heat transfer efficiency at fixed buoyancy forces, while changing the concentration $\Phi_0$ of the emulsions, from the dilute to the moderately concentrated regimes. The temperature field is shown in simulation units.

## II. NUMERICAL METHODS

We employ a mesoscopic approach to simulate thermal convection in stabilised emulsions, by coupling a lattice Boltzmann method (LBM) [58, 59] for non-ideal multicomponent mixtures with an LBM for the temperature field dynamics. We briefly report the essential information about the two LB formulations, referring to other specific works [26, 60–64] for more technical details.

The emulsion is simulated with two components (say $A$ and $B$) LBM. The model hinges on the dynamical evolution of mesoscopic probabilities density functions $f_\ell^i(\boldsymbol{x},t)$ of finding a particle of component $\ell = A, B$ in the space-time location $(\boldsymbol{x},t)$ with lattice velocity $\boldsymbol{c}^i$, where the index $i$ takes only a finite number of values. We employ a D2Q9 scheme, with 9 lattice velocities in a two-dimensional domain. The dynamical evolution of the distribution functions embeds streaming steps supplemented with local collisions. This translates into the following evolution over a unitary time lapse $\Delta t = 1$

$$f_\ell^i(\boldsymbol{x}+\boldsymbol{c}^i,t+1)-f_\ell^i(\boldsymbol{x},t) = -\frac{1}{\tau}\left(f_\ell^i - f_\ell^{(eq,i)}\right)(\boldsymbol{x},t)+F_\ell^i(\boldsymbol{x},t) \tag{1}$$

where $\tau$ is a relaxation time towards the local equilibrium $f_\ell^{(eq,i)}$ (repeated indices are summed upon)

$$f_\ell^{(eq,i)} = w_i\rho_\ell\left[1+\frac{u_k c_k^i}{c_s^2}+\frac{u_k u_p(c_i^k c_i^p - c_s^2\delta_{kp})}{2c_s^4}\right]$$

where $w_i$ are suitable weights and $c_s^2 = 1/3$ is a constant in the model. The density fields $\rho_\ell(\boldsymbol{x},t) = \sum_i f_\ell^i(\boldsymbol{x},t)$ ($\ell$=$A$, $B$) and the global momentum field $\rho\boldsymbol{u}(\boldsymbol{x},t) = \sum_{\ell,i}\boldsymbol{c}_i f_\ell^i(\boldsymbol{x},t)$, with $\rho = \sum_\ell \rho_\ell$, are coarse-grained fields suitably constructed from the distribution functions. The source term $F_\ell^i(\boldsymbol{x},t)$ includes the effects of interaction (int) forces, $\boldsymbol{F}_{\rm int}(\boldsymbol{x},t)$, and external (ext) volume forces, $\boldsymbol{F}_{\rm ext}(\boldsymbol{x},t)$. Interaction forces are chosen in such a way that phase separation is triggered between the two components, so that the formation of stable interfaces separating bulk regions (with majority of one component) is formed. Simultaneously, competing interaction forces are also introduced at the interfaces to inhibit droplets coalescence [60, 65–67]. This combination makes possible the simulation of a given number of droplets of the dispersed phase (A) into the continuous phase (B). All technical details on the interaction forces can be found in dedicated papers [26, 60, 62–64]. Regarding the external volume forces, a buoyancy term is added to the global momentum balance in the Boussinesq's form $\boldsymbol{F}_{\rm ext}(\boldsymbol{x},t) = \rho(\boldsymbol{x},t)\,\alpha\,g\,T(\boldsymbol{x},t)\,\boldsymbol{e}_y$, where $T(\boldsymbol{x},t)$ is the temperature field relative to some reference temperature, $\alpha$ the thermal expansion coefficient, $g$ the gravity acceleration and $\boldsymbol{e}_y$ the unit vector in the wall-to-wall direction. At large scales, the long wavelength limit of the lattice Boltzmann model maps into the diffuse-interface Navier-Stokes equations [58, 59]

$$\begin{aligned}\rho\left(\partial_t + u_k^{(\rm H)}\partial_k\right)u_i^{(\rm H)} = &+\partial_j\left[-P_{ij}+\eta_0\left(\partial_i u_j^{(\rm H)}+\partial_j u_i^{(\rm H)}\right)\right]\\ &+\rho\alpha g T\delta_{iy} \qquad i=x,y\end{aligned} \tag{2}$$

where $\rho\boldsymbol{u}^{(\rm H)} = \rho\boldsymbol{u}+\boldsymbol{F}_{\rm int}/2+\boldsymbol{F}_{\rm ext}/2$ is the hydrodynamical momentum of the mixture. The non-ideal pressure tensor $P_{ij}$ is non-diagonal due to the contribution of interaction forces [68, 69]. The bulk viscosity $\eta_0$ is linked to the relaxation time $\tau$ of the lattice Boltzmann according to the following relation:

$$\eta_0 = \rho c_s^2(\tau - 1/2). \tag{3}$$

Hence, $\eta_0$ can be tuned via a proper choice of the relaxation time in the lattice Boltzmann dynamics (1). The boundary conditions for the hydrodynamical fields correspond to a no-slip at the walls, which we achieve with suitable bounce-back rules [58, 59] implemented at the level of the distribution functions. Periodic boundary conditions are applied in the $x$-direction.

The evolution of the temperature field $T(\boldsymbol{x},t)$ is integrated via another properly devised lattice Boltzmann scheme [61]. In a nutshell, we evolve in time an auxiliary probability distribution function $g^i(\boldsymbol{x},t)$, whose coarse-grained counterpart is the temperature field. i.e. $T(\boldsymbol{x},t) = \sum_i g^i(\boldsymbol{x},t)$. The mesoscopic dynamics for $g^i(\boldsymbol{x},t)$ reads as follow:

$$g^i(\boldsymbol{x}+\boldsymbol{c}_i,t+1)-g^i(\boldsymbol{x},t) = -\frac{1}{\tau_g}\left(g^i - g^{(eq,i)}\right)(\boldsymbol{x},t) \quad (4)$$

where the local equilibrium $g^{(eq,i)}$ takes now the form

$$g^{(eq,i)} = w_i \rho_\ell \left[1 + \frac{u_k^{(\mathrm{H})} c_k^i}{c_s^2} + \frac{u_k^{(\mathrm{H})} u_p^{(\mathrm{H})}(c_i^k c_i^p - c_s^2 \delta_{kp})}{2c_s^4}\right].$$

The long-wavelength limit of (4) approximates the advection-diffusion equation for the temperature field

$$\partial_t T + u_k^{(\mathrm{H})} \partial_k T = \kappa \partial_{kk} T \quad (5)$$

where $\kappa = c_s^2(\tau_g - 1/2)$ is the thermal diffusivity which can be tuned by changing the thermal relaxation time $\tau_g$. The advection-diffusion equation (5) is two-way coupled with the Navier-Stokes equation (2): i) via the fluid velocity field entering the advection term in (5) and ii) via the buoyancy force in the r.h.s. of (2). The boundary conditions for the temperature field are of Dirichlet type, i.e. we prescribe constant temperatures $T(x, y = \pm H/2, t) = \mp \Delta T/2$, with $\Delta T = 1.0$ lattice simulation units (lbu), at the upper and lower walls, respectively, whereas we apply periodic boundary conditions in the $x$-direction. Notice that all dimensional observables will be reported in simulation units (i.e. lattice Boltzmann units, lbu). The software we employ for all the simulations is an extension of an in-house developed code written in C-CUDA. The code has been described in detail elsewhere [70]. Here we recall just that it exploits at its best the computing power of modern Graphics Processing Units (GPU) by means of an innovative memory access pattern. The code is able to run on multiple GPUs. To that purpose we resort to a hybrid parallel programming model (based on a combination of MPI and CUDA). The smoothness by which the thermal LB component has been implemented confirms the flexibility of the software that, in addition, supports a number of different boundary conditions and the chance of simulating the presence of obstacles within the computational domain [26, 71, 72].

## III. RESULTS AND DISCUSSION

We numerically study the heat transfer properties of emulsions. To this aim, we perform simulations by placing the emulsions in a channel of height $H \sim 17d$, where $d$ is the mean droplet diameter, and we systematically explore different droplet concentrations $\Phi_0$, from very diluted to concentrated emulsions, by varying the number of droplets $N_{\mathrm{droplets}}$ (see Table I). In order to assess the heat transfer properties of the emulsion, we focus on the heat flux across the system, $\mathcal{F}$, which is the sum of a conductive and a convective part, $\mathcal{F} = \mathcal{F}_{\mathrm{cond}} + \mathcal{F}_{\mathrm{conv}}$; both can, in principle, differ in the biphasic system, from the mono-phasic counterpart. For our simulations, the two fluids have the same thermal diffusivity and no interfacial thermal resistance is supported, therefore $\mathcal{F}_{\mathrm{cond}}$ is not affected. The presence of the dispersed phase (see Fig. 1 for a pictorial view of how the system looks like at different concentrations), instead, is known to alter the rheology of the mixture (with respect to a situation with a pure solvent), and, hence, also its convective heat transfer properties. The droplet concentration $\Phi_0$ is the ratio of the volume of dispersed phase over the total volume, $\Phi_0 = \mathcal{V}_d/\mathcal{V}_t$; such a definition surmises, of course, a sharp interface. Since we use a diffuse interface method, we need to introduce a threshold, $\rho^*$, on the density, to define the droplet volume, that is $\mathcal{V}_d = \int\int \Theta(\rho_A(x,y) - \rho^*) dx\ dy$, where $\Theta$ is the Heaviside step function. A natural choice for $\rho^*$ is the mean density of the dispersed phase in the bulk phase, i.e. $\rho^* = (\rho^{\max}_{A,\mathrm{bulk}} + \rho^{\min}_{A,\mathrm{bulk}})/2$. In Fig. 2 we show the flow curves (panel (a)), and the effective viscosity (panel (b)) for various concentrations of the emulsions. The flow curves are obtained from homogeneous shear simulations, where constant and opposite velocities are imposed at the walls ($u_x^{\mathrm{wall}}(y = \pm H/2, t) = \pm U$); given the flow curve data, the effective viscosity is measured as the ratio between shear stress and shear rate, $\eta_{\mathrm{eff}} = d\Sigma/d\dot{\gamma}$. At low droplet concentrations, the dispersion behaves as a Newtonian fluid, with an augmented effective viscosity [73, 74]: dark region in Fig. 2(b) (and hereafter) shows the range in which non-Newtonian effects start to emerge. Let us recall that for suspensions of solid spherical particles, in the very dilute limit ($\Phi_0 \to 0$), Einstein predicted a linear growth of the relative viscosity with $\Phi_0$ [75]; later on, G.I. Taylor proved that linearity holds also for the relative viscosity of three-dimensional emulsions [16] (in the small droplet deformation regime), i.e.:

$$\eta_r(\Phi_0) \equiv \frac{\eta_{\mathrm{eff}}(\Phi_0)}{\eta_{\mathrm{solv}}} = 1 + [\eta]_0 \Phi_0, \quad (6)$$

with an intrinsic viscosity coefficient dependent on the viscosity ratio $\lambda$ as $[\eta]_0 = \frac{\frac{5}{2}\lambda+1}{\lambda+1}$ (which tends to 5/2, the Einstein's coefficient for solid particles, as $\lambda \to \infty$). In Fig. 3 we show $\eta_r$ as a function of $\Phi_0$ for the emulsion.

| $\Phi_0$ | $N_{\mathrm{droplets}}$ | $\Phi_0$ | $N_{\mathrm{droplets}}$ |
|---|---|---|---|
| 0.0735 | 90 | 0.2357 | 242 |
| 0.1038 | 120 | 0.2680 | 284 |
| 0.1433 | 159 | 0.3322 | 338 |
| 0.1721 | 214 | 0.3978 | 392 |
| 0.2018 | 235 | 0.4775 | 449 |

TABLE I. Number of droplets $N_{\mathrm{droplets}}$ simulated for each concentration $\Phi_0$.

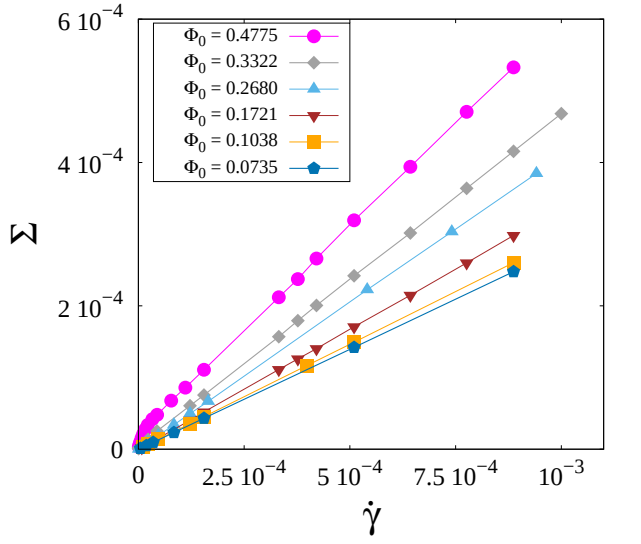


(a)

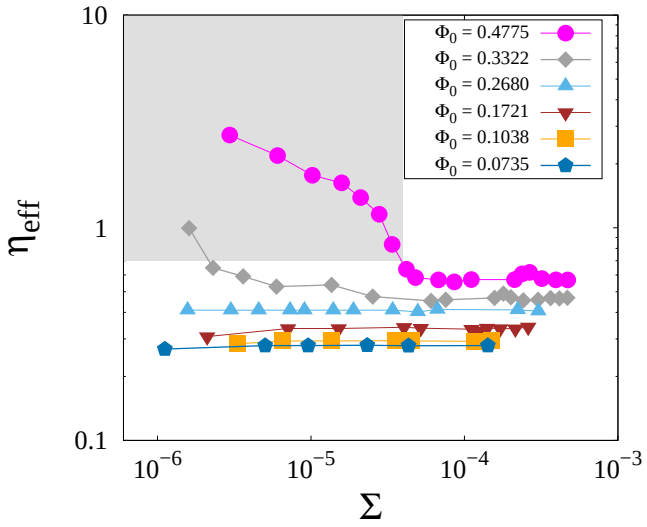


(b)

FIG. 2. Shear rheology of the emulsions. Panel (a): flow curves for the emulsion systems obtained with dedicated shear experiments (see text for details). The concentration is varied. Panel (b): the emulsion effective viscosity $\eta_{\rm eff}$ as a function of shear stress $\Sigma$, extracted from the flow curves in panel (a), for different concentrations [10]. The dark region refers to a range of concentrations for which non-Newtonian effects start to emerge. All dimensional quantities are reported in simulation units.

The measured relative viscosity is in good agreement with Eq. (6), with $[\eta]_0 = 7/4$, as expected for an emulsion with unitary viscosity ratio ($\lambda = 1$), for concentrations up to $\Phi_0 \approx 0.12$. The agreement is improved upon using a 2D estimate of the effective viscosity, that we have extracted from the data in [36], as we can see in the zoom-in reported in the inset. At larger droplet concentrations, data start to deviate from dilute predictions. Specifically, for larger $\Phi_0$ (and up to $\Phi_0 \approx 0.35$) our data agree well

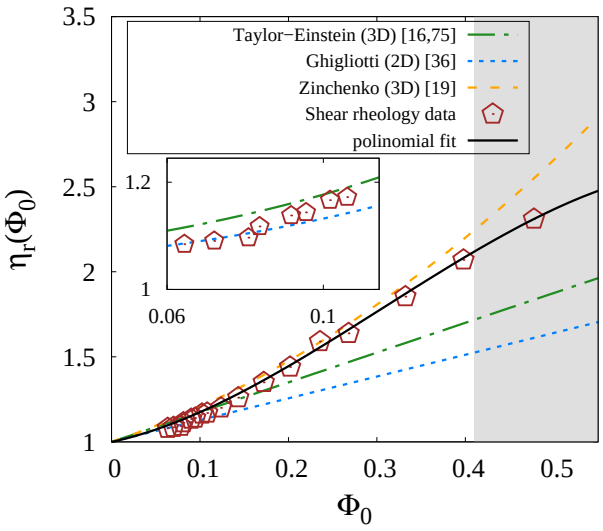


FIG. 3. We report the intrinsic viscosity $\eta_r(\Phi_0)$ (cfr. Eq. (6)) for the shear rheology data of panel (a) of Fig. 2, along with its best polynomial fit which well approximates the data at all concentration studied. We also report literature estimates for the effective viscosity, both in a 2D and in a 3D set-up. In the inset, we zoom-in at very low $\Phi_0$ to highlight the agreement with [36] up to $\Phi_0 \approx 0.12$. The dark region refers to a range of concentrations for which non-Newtonian effects start to emerge (cfr. Fig. 2). All dimensional quantities are reported in simulation units.

with Zinchenko's prediction for three-dimensional emulsions [19]. An obvious effect of increasing the concentration is to increase the system viscosity, thereby reducing its propensity to convection. One would expect simply a monotonic decay of the heat flux with $\Phi_0$. Actually, the phenomenology is more complicated, as shown in Fig. 4, where we analyse the heat fluxes, expressed in a dimensionless form via the Nusselt number [54, 57, 76, 77]

$$\mathrm{Nu}(t) = \frac{\langle u_y(x,y,t)T(x,y,t)\rangle_{x,y} - \kappa\langle \partial_y T(x,y,t)\rangle_{x,y}}{\kappa\frac{\Delta T}{H}} \tag{7}$$

where $\langle(\dots)\rangle_{x,y}$ denotes a space average. In Fig. 4(a) we report $\mathrm{Nu}(t)$ for different values of $\Phi_0$, at fixed buoyancy amplitude $\alpha g \Delta T = 1.86\ 10^{-5}$ lbu; the time average of $\mathrm{Nu}(t)$ over the statistically steady-state ($\langle \mathrm{Nu}\rangle_t$) is reported in Fig. 4(b), while fluctuations around the mean ($\Delta\mathrm{Nu} = \langle(\mathrm{Nu}(t) - \langle \mathrm{Nu}\rangle_t)^2\rangle_t^{1/2}$) are displayed in the inset of the panel (b) as a function of $\Phi_0$. We observe that $\langle \mathrm{Nu}\rangle_t$ stays nearly constant for concentrations up to $\Phi_0 \approx 0.2$, whereas the fluctuations $\Delta\mathrm{Nu}$ tend to increase with $\Phi_0$. In particular, in the limit $\Phi_0 \to 0$, i.e. for a single-phase (SP) system, the fluctuations go to zero, indicating that the convection is stationary (dashed black line in Fig. 4), by reason of a relatively low Rayleigh num-

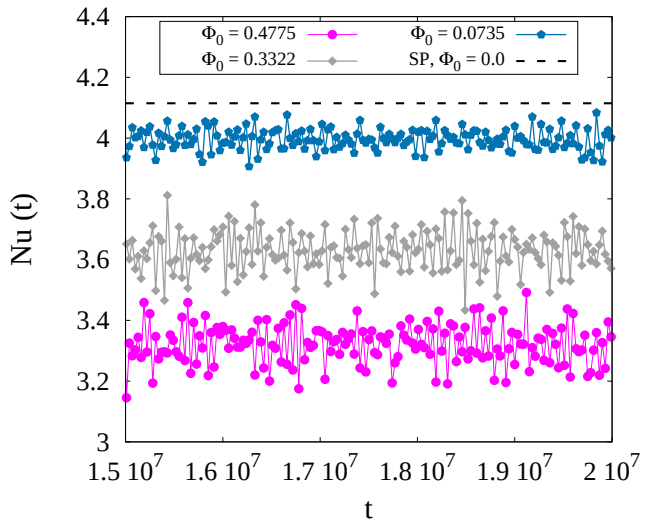


(a)

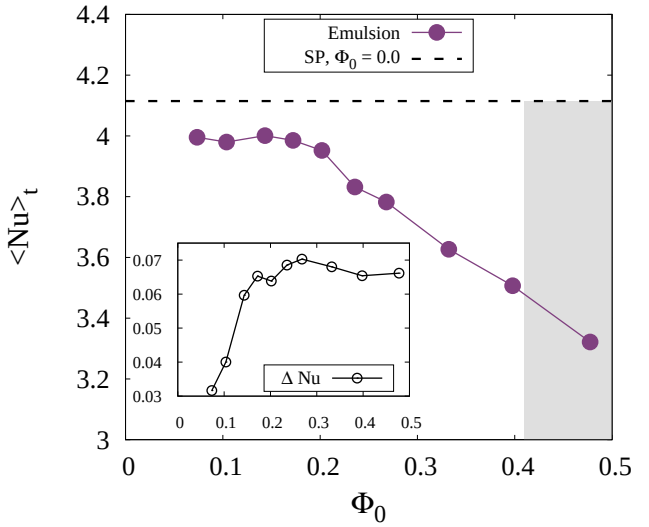


(b)

FIG. 4. Panel (a): Nusselt number as a function of time $t$ (cfr. Eq. (7)) for different concentrations $\Phi_0$. The magnitude of buoyancy forces is kept fixed. The dashed line represents the corresponding Nusselt number for a single-phase (SP) system ($\Phi_0 \to 0$). Panel (b): We report the time-averaged of the Nusselt number $\langle \mathrm{Nu} \rangle_t$. In the inset, we report Nusselt number fluctuations around the mean value, $\Delta \mathrm{Nu} = \langle (\mathrm{Nu}(t) - \langle \mathrm{Nu} \rangle_t)^2 \rangle_t^{1/2}$. The dark region refers to a range of concentrations for which non-Newtonian effects start to emerge (cfr. Fig. 2). All dimensional quantities are reported in simulation units.

ber, $Ra \approx 5.3 \times 10^4$ [53] [1] The emergence of fluctuations must then be interpreted as a genuine feature of the heterogeneous system and it is ascribed to the presence of the droplet phase. In what follows, we investigate on the time-averaged Nusselt number $\langle \mathrm{Nu} \rangle_t$, leaving the study of the origin and statistical properties of the fluctuations to a separated dedicated study [78].

To delve deeper into the behaviour of $\langle \mathrm{Nu} \rangle_t$ with increasing droplet concentration, the natural question is whether one might capture it by means of a continuum approach. For this purpose, we ran simulations with the SP system with a homogeneous viscosity equal to the shear viscosity that we have measured (cfr. Fig. 2(b)), i.e.

$$\eta^{\mathrm{SP}}_{\mathrm{rheo}}(\Phi_0) = \eta_{\mathrm{eff}}(\Phi_0). \tag{8}$$

This is possible within our numerical approach, by changing the relaxation time of the lattice Boltzmann equation in such a way that the corresponding dynamic viscosity (cfr. Eq.(3)) matches the measured shear viscosity *homogeneously* throughout the system. Notice that SP systems constructed in that way, exhibit a Nusselt number independent of time, for the reasons posited before. In Fig. 5 we report the time-averaged Nusselt number $\langle \mathrm{Nu} \rangle_t$ as a function of the droplet concentration $\Phi_0$ for both the heterogeneous emulsions and the homogeneous SP system. In the limit $\Phi_0 \to 0$ the time-averaged Nusselt numbers tend to coincide, as they should. At increasing $\Phi_0$, the Nusselt number measured in the SP simulations decreases monotonically, as expected for an increasingly viscous system. Therefore, we observe a mismatch with the behaviour of $\langle \mathrm{Nu} \rangle_t$ in the emulsion case, which becomes particularly evident (with deviations up to roughly 10%) for intermediate values of the concentration and then decreases again at larger $\Phi_0$. Even if the two curves seem to join at $\Phi_0 = 0.4775$, this is not true for $\Phi_0 \geq 0.5$: further increasing the droplet concentration, the heat flux (i.e. the Nusselt number) is more and more inhibited for emulsion, whereas in the homogeneous case a sort of plateau is reached (data not shown). This disagreement is caused by the predominance of non-Newtonian effects, whose analysis departs from the scope of this paper (a step in this direction has been taken in [78]). The assumption of a global effective viscosity equal to the one extracted from the shear rheology, is clearly not enough. In order to gain a better insight, it is worth reminding that for the thermal convection in a different soft system (polymer solutions), it was shown that variation in the heat flux could be understood in terms of a space-dependent effective viscosity (due, in that case, to the differential stretching of the polymers along with the cell height) [79]. Inspired by this observation, we inspected whether a *local* effective viscosity should be considered in our case as well, due to, e.g., a non-homogeneous droplet distribution across the system. For this purpose, we monitored the droplet concentrations in the wall-to-wall coordinate ($y$), by averaging over time and along the mainstream flow direction ($x$). The resulting concentration profiles $\phi_0(y)$ are reported in Fig. 6. We observe, indeed, they are not constant

[1] The Rayleigh number $Ra$ is defined as $Ra = \frac{g\alpha \Delta T H^3}{\kappa \nu}$, where $\nu$ is the kinematic viscosity. It provides information on the balance between buoyancy force and viscous friction force.

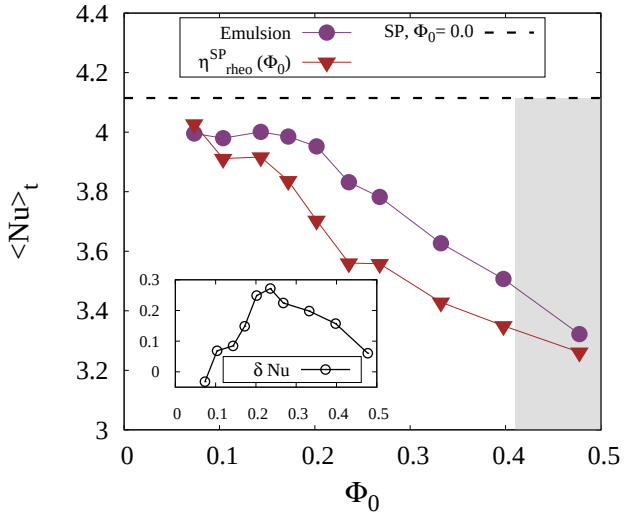


FIG. 5. The time-averaged Nusselt number $\langle \mathrm{Nu} \rangle_t$ as a function of the concentration $\Phi_0$ for two different cases: emulsion (purple circles) and a single-phase system (SP, brown triangles) with a dynamic viscosity that homogeneously matches the rheological viscosity (cfr. Eq. (8) and Fig. 2). The dark region refers to a range of concentrations for which non-Newtonian effects start to emerge (cfr. Fig. 2). The comparison, exalted by $\delta\mathrm{Nu} = \langle \mathrm{Nu} \rangle_t - \mathrm{Nu}^{\mathrm{SP}}_{\mathrm{rheo}}$, is given in the inset.

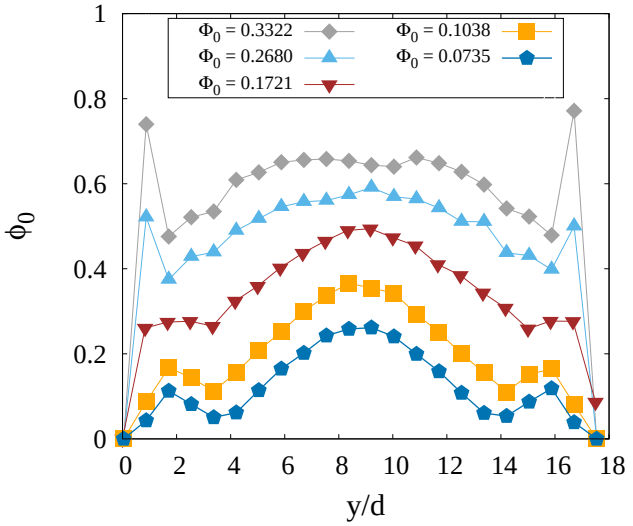


FIG. 6. Concentration profiles $\phi_0(y)$. The $y$ coordinate is normalised to the mean droplet diameter $d$. Each color/symbol is associated with a different concentration $\Phi_0$.

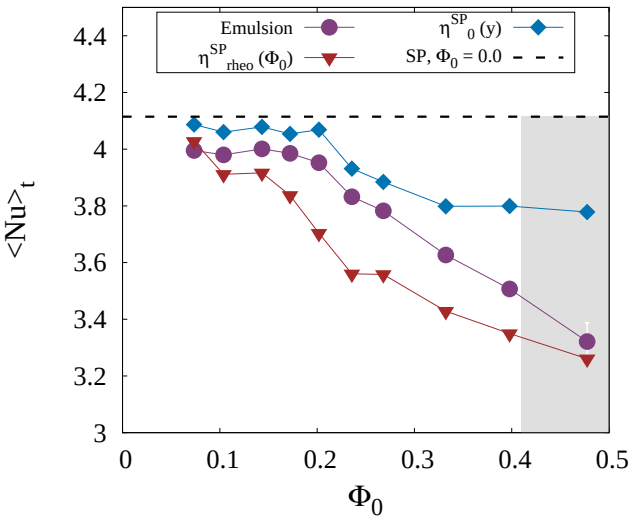


FIG. 7. We report data given in Fig. 5 with the additional plot of the time-averaged Nusselt number $\langle \mathrm{Nu} \rangle_t$, as a function of $\Phi_0$, obtained with a local viscosity $\eta_0^{\mathrm{SP}}(y)$ given by (9). The dark region refers to a range of concentrations for which non-Newtonian effects start to emerge (cfr. Fig. 2).

and exhibit a height-varying modulation, especially from low to moderate concentrations $\Phi_0$. The development of these non-homogeneous concentration profiles might be due to multiple factors, such as droplet migration induced by a non-uniform shear field [80–82] (owing to the large scale circulation of convection) or droplet depletion due to interactions with the walls. A precise description disentangling these various mechanisms and discriminating which one contributes most, lies beyond the scope of the present work. Here, just take the emergence of such profiles as an empirical fact. This said it is nevertheless clear that the non-homogeneity relies on the fact that droplets are transported by the flow. Large $\Phi_0$ implies reduced mobility of the droplets, which is reflected in a relative suppression of profile modulation. To account for this aspect in the SP fluid model, we promote the effective viscosity to be a local quantity as well, i.e.

$$\eta_0^{\mathrm{SP}}(y) = f(\phi_0(y)), \tag{9}$$

where the function corresponds to the fit displayed in Fig. 3 (black solid line). In Fig. 7, the Nusselt number obtained from SP simulations with the prescription (9) are compared with the $\langle \mathrm{Nu} \rangle_t$ vs $\Phi_0$ data for the emulsions reported in Fig. 5. A first remark to be raised is that the emulsions data stay in between the two protocols: while the protocol (8) underestimates the emulsions data, the new protocol (9) overestimates them. A possible explanation for the deviations observed in comparing the emulsions data with the protocol (9) can be grasped by looking at the concentration profiles for the largest $\Phi_0$ in Fig. 6; the latter are basically flat, but for an overshooting occurring in the wall-proximal regions whose extension is comparable to $1-2$ droplet sizes (droplet layering). Forcing the continuum model SP fluid to vary its properties (effective viscosity) over such a micro-constituent size may then lead to artefacts. To overcome this problem, we propose to generalise the local effective viscosity (9) as follows:

$$\eta_\Lambda^{\mathrm{SP}}(y) = f(\phi_\Lambda(y)), \tag{10}$$

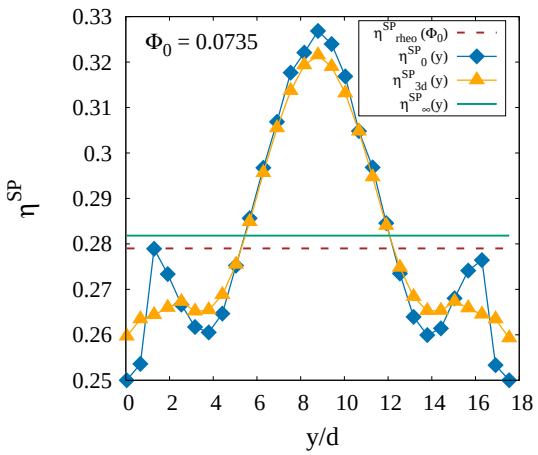


(a)

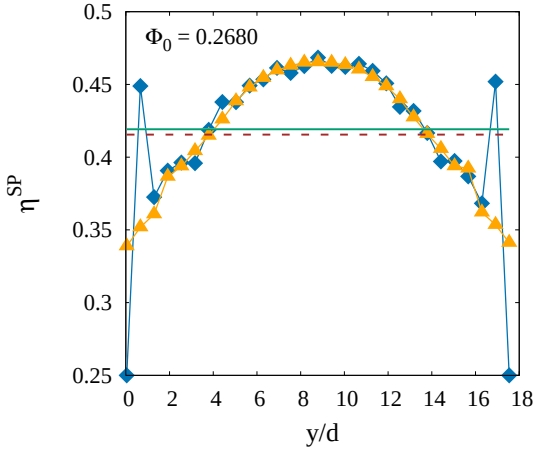


(b)

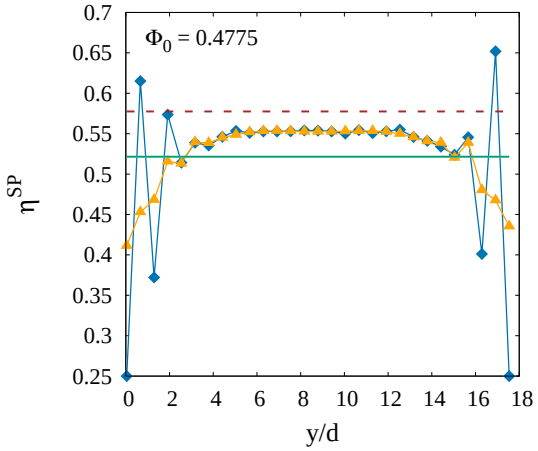


(c)

FIG. 8. Viscosity profiles $\eta^{\rm SP}(y)$ for three different concentrations $\Phi_0$: $\Phi_0 = 0.0735$ (Panel (a)), $\Phi_0 = 0.2680$ (Panel (b)) and $\Phi_0 = 0.4775$ (Panel (c)). Predictions for $\eta^{\rm SP}_{\rm rheo}(\Phi_0)$ from protocol Eq. (8) are compared with predictions $\eta^{\rm SP}_{\Lambda}(y)$ from protocol Eq. (10) using various resolutions of the coarse-graining parameter $\Lambda$ (cfr. Eq. (11)). The $y$-coordinate is normalised by the mean droplet diameter $d$. All dimensional quantities are reported in simulation units.

where $\phi_\Lambda(y)$ is a *coarse-grained* (over a size $\Lambda$) concentration profile defined as:

$$\phi_\Lambda(y) = \frac{1}{\Lambda}\int_{y-\Lambda/2}^{y+\Lambda/2} \phi_0(y')dy'. \qquad (11)$$

Notice that for $\Lambda = 0$ the original concentration profile $\phi_0(y)$ is recovered, by definition. Fig. 8 shows the results of this procedure on $\eta^{\rm SP}_\Lambda(y)$ for $\Lambda = 0, 3d$ and $\Lambda \to \infty$ (corresponding to a constant effective viscosity) and for three values of $\Phi_0$ (the values of $\eta^{\rm SP}_{\rm rheo}(\Phi_0)$ are also reported for comparison). The oscillations near the walls, stemming from the droplet layering, are smoothed out, highlighting that the relative variation of the effective viscosity is actually more important for the lower concentrations (panels (a) and (b)). Simulating the SP fluid with the choice (10) for the effective viscosity, indeed, yields the best agreement with the phenomenology of the emulsion in terms of the time-averaged heat flux $\langle {\rm Nu}\rangle_t$, as shown in Fig. 9, for $\Lambda = 3d$ (we also plot the data for $\Lambda \to \infty$ which, not surprisingly, basically overlap with those for $\eta^{\rm SP}_{\rm rheo}(\Phi_0)$). However, a mismatch between the two curves, emulsion and SP system with $\eta^{\rm SP}_{3d}(y)$, occurs whenever the concentration is sufficiently high to trigger non-Newtonian effects. This non-Newtonian behaviour, which is inherent to the nature of systems, promotes the onset of highly viscous regions where heat transfer is to large extent suppressed. In this case, it becomes difficult to reproduce the SP system with the same heat transfer as the highly concentrated emulsion, based on the protocol (10); rather, it is necessary to consider the extra complication of a shear-dependent viscosity and study the associated non-local effects, as discussed in [78].

As mentioned above, the results obtained so far refer to a fixed buoyancy amplitude $\alpha g \Delta T = 1.86\ 10^{-5}$ lbu (i.e. at fixed Rayleigh number $Ra$). It appears then natural to investigate the impact of changing the value of $\alpha g \Delta T$ on the protocol (10). To this aim, we have performed additional numerical simulations at different buoyancy amplitude $\alpha g \Delta T$ and compared the time-averaged Nusselt number $\langle {\rm Nu}\rangle_t$ obtained from simulations of the emulsions at changing $\Phi_0$, with that of SP system with viscosity given by (10). Results are reported in Fig. 10, which displays a satisfactory agreement between the numerical simulations and protocol (10) for $\alpha g \Delta T$ spanning an order of magnitude, from $\alpha g \Delta T = 6.21\ 10^{-6}$ lbu to $\alpha g \Delta T = 1.86\ 10^{-5}$ lbu. Because of the coalescence of the droplets, larger values of the buoyancy amplitude $\alpha g \Delta T$ could not be explored in detail.

## IV. CONCLUSIONS

We have analysed the heat transfer properties of concentrated emulsions just above the onset of convection, by means of extensive mesoscale simulations. The droplet concentrations $\Phi_0$ in the emulsions have been chosen to range systematically from very dilute situations to

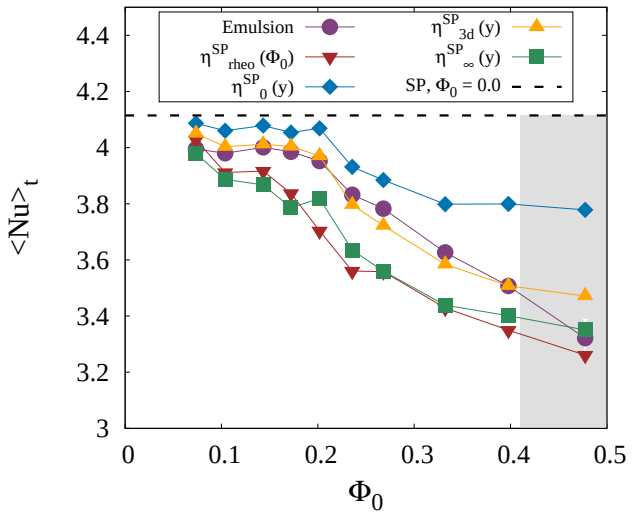


FIG. 9. The time-averaged Nusselt number $\langle \mathrm{Nu} \rangle_t$ as a function of concentration $\Phi_0$ for emulsion (purple circles) and a single-phase system (SP) with different choices of the viscosity $\eta^{\mathrm{SP}}$ (other colours/symbols). We report data based on $\eta^{\mathrm{SP}}_{\mathrm{rheo}}(\Phi_0)$ from protocol Eq. (8) and data based on $\eta^{\mathrm{SP}}_{\Lambda}(y)$ from protocol Eq. (10) using various resolutions of the coarse-graining parameter $\Lambda$ (cfr. Eq. (11). The dark region refers to a range of concentrations for which non-Newtonian effects start to emerge (cfr. Fig. 2).

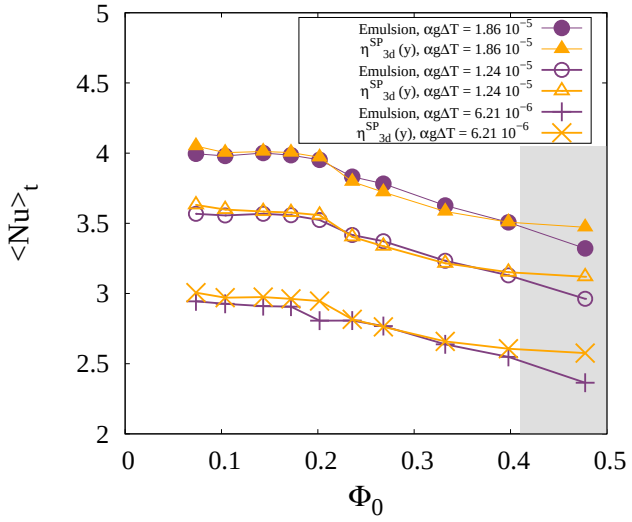


FIG. 10. The time-averaged Nusselt number $\langle \mathrm{Nu} \rangle_t$ as a function of the concentration $\Phi_0$: comparison between emulsion (purple points: full circles, empty circles, daggers) and single-phase system (SP, orange points: full triangles, empty triangles, times symbols) with a resolution of coarse-graining process $\Lambda = 3d$, for different applied buoyancy force $\alpha g$ in Eq. (2). The dark region refers to a range of concentrations for which non-Newtonian effects start to emerge (cfr. Fig. 2).

situations with larger concentrations, around the point the emulsion stops behaving as a Newtonian fluid. We explored the heat transfer properties while keeping the droplet size finite, thus disclosing insights into the way a continuum picture (i.e. point-like droplets) is changed by the finite-size effects induced by a non-zero extension of the droplets. We find that the heat transport efficiency (i.e. the Nusselt number) displays a non-stationary character in time, while its time-average decreases at increasing $\Phi_0$. In the attempt of capturing the time-averaged Nusselt number $\langle \mathrm{Nu} \rangle_t$ at changing droplet concentration $\Phi_0$, we pursued the idea of considering a single-phase (SP) system, equipped with a suitable choice of viscosity $\eta^{\mathrm{SP}}$ that allows the SP system to display (on average) the same heat transport efficiency of the emulsions. Specifically, starting from the knowledge of the shear rheology for the emulsions $\eta_{\mathrm{eff}}(\Phi_0)$, we investigated the suitable protocol that allows constructiong $\eta^{\mathrm{SP}}$. Due to the convective dynamics, the emulsion develops a non-homogeneous droplet distribution across the cell, implying that any choice of $\eta^{\mathrm{SP}}$ must be local, i.e. acquire a space-dependence. Moreover, a quantitative analysis reveals that this local viscosity must be properly supplemented with a spatial averaging procedure ("coarse-graining"), over a scale that is of the order of the droplet size.

For the future, various pathways are worth being pursued. As previously discussed, the coarse-graining procedure presented in this paper does not represent the end of the story: as a matter of fact, although it works well in reproducing the behaviour of the time-averaged Nusselt number, the fluctuations around that mean value are not retained in the SP systems. The correct way to capture those temporal fluctuations is not clear at this stage: they can be measured and characterised in the simulations with the emulsions, but the specific way to embed them in a continuum approach warrants a dedicated study. Moreover, in this paper, we deliberately studied emulsion concentrations that result only in Newtonian responses. Further increasing the droplet concentration would produce a non-Newtonian emulsion. A recent complementary study indeed reveals that, under those conditions, fluctuations in the Nusselt number are even more abrupt than those observed at the smaller concentrations and they are further accompanied by the emergence of space correlations and "bursts" of enhancement in the local heat transport [78].

Overall, all these observations suggest that any approach aiming at a quantitative description of heat transfer in fluid-fluid dispersions must take into account the discrete nature of such complex fluids.

## ACKNOWLEDGEMENTS

Funding support to lead these results was received from the European Research Council under the Horizon 2020 Programme Grant Agreement n. 739964 ("COPMAT"). The authors acknowledge Prof. Giacomo Falcucci, Dr. Fabio Bonaccorso for useful support.

Some of the simulations were performed on Jeeg, the graphical-accelerated facility of the University of Naples "Parthenope". Jeeg was acquired with the Italian Government Grant PAC01_00119 MITO "Informazioni Multimediali per Oggetti Territoriali", with Prof. Elio Jannelli as the principal investigator.

* francesca.pelusi@roma2.infn.it

[1] G. Hetsroni, *Handbook of multiphase systems*, McGraw-Hill Book Co., New York, NY, 1982.
[2] A. Faghri and Y. Zhang, in *Fundamentals of Multiphase Heat Transfer and Flow*, Springer, 2020, pp. 257–321.
[3] S. W. Kim, J. Y. Ahn, S. D. Kim and D. H. Lee, *International Journal of Heat and Mass Transfer*, 2003, **46**, 399–409.
[4] P. Oresta, R. Verzicco, D. Lohse and A. Prosperetti, *Phys. Rev. E*, 2009, **80**, 026304.
[5] L. E. Schmidt, P. Oresta, F. Toschi, R. Verzicco, D. Lohse and A. Prosperetti, *New Journal of Physics*, 2011, **13**, 025002.
[6] R. Nigmatulin, A. Filippov and A. Khismatullin, *Thermophysics and aeromechanics*, 2012, **19**, 589–606.
[7] R. Lakkaraju, R. J. A. M. Stevens, P. Oresta, R. Verzicco, D. Lohse and A. Prosperetti, *Proceedings of the National Academy of Sciences*, 2013, **110**, 9237–9242.
[8] S. Yao and K. Choit, *International Journal of Multiphase Flow*, 1987, **13**, 639–648.
[9] L. Royon and G. Guiffant, *Energy Conversion and Management*, 2001, **42**, 2155–2161.
[10] R. Pal, *Journal of colloid and interface science*, 2000, **225**, 359–366.
[11] J. Shao, J. Darkwa and G. Kokogiannakis, *Energy and buildings*, 2015, **94**, 200–217.
[12] F. Wang, W. Lin, Z. Ling and X. Fang, *Solar Energy Materials and Solar Cells*, 2019, **191**, 218–234.
[13] S. Shin and S.-H. Lee, *International journal of heat and mass transfer*, 2000, **43**, 4275–4284.
[14] A. Guha, *Annu. Rev. Fluid Mech.*, 2008, **40**, 311–341.
[15] M. Niazi Ardekani, O. Abouali, F. Picano and L. Brandt, *Journal of Fluid Mechanics*, 2018, **834**, 308–334.
[16] G. I. Taylor, *Proceedings of the Royal Society of London. Series A, Containing Papers of a Mathematical and Physical Character*, 1932, **138**, 41–48.
[17] N. Frankel and A. Acrivos, *Journal of Fluid Mechanics*, 1970, **44**, 65–78.
[18] D. Barthes-Biesel and A. Acrivos, *Journal of Fluid Mechanics*, 1973, **61**, 1–22.
[19] A. Zinchenko, *Journal of Applied Mathematics and Mechanics*, 1984, **48**, 198–206.
[20] H. Princen, *J. Colloid Interface Sci.*, 1983, **91**, 160 – 175.
[21] C. Pozrikidis, *Journal of Fluid Mechanics*, 1990, **210**, 1–21.
[22] P. Maffettone and M. Minale, *Journal of Non-Newtonian Fluid Mechanics*, 1998, **78**, 227–241.
[23] M. Loewenberg and E. Hinch, *Journal of Fluid Mechanics*, 1996, **321**, 395–419.
[24] J. Rallison and A. Acrivos, *Journal of Fluid Mechanics*, 1978, **89**, 191–200.
[25] J. Rallison, *Journal of Fluid Mechanics*, 1981, **109**, 465–482.
[26] A. Scagliarini, M. Lulli, M. Sbragaglia and M. Bernaschi, *Europhys. Lett.*, 2016, **114**, 64003.
[27] T. Mason, J. Bibette and D. Weitz, *Journal of colloid and interface science*, 1996, **179**, 439–448.
[28] S. Guido and M. Villone, *Journal of rheology*, 1998, **42**, 395–415.
[29] V. Sibillo, G. Pasquariello, M. Simeone, V. Cristini and S. Guido, *Physical review letters*, 2006, **97**, 054502.
[30] N. Vankova, S. Tcholakova, N. D. Denkov, I. B. Ivanov, V. D. Vulchev and T. Danner, *Journal of Colloid and Interface Science*, 2007, **312**, 363–380.
[31] H. A. Barnes, *Colloids and Surfaces A: Physicochemical and Engineering Aspects*, 1994, **91**, 89–95.
[32] R. Pal, *AIChE Journal*, 1996, **42**, 3181–3190.
[33] T. Mason, *Current Opinion in Colloid & Interface Science*, 1999, **4**, 231–238.
[34] S. R. Derkach, *Advances in colloid and interface science*, 2009, **151**, 1–23.
[35] T. F. Tadros, *Emulsion formation and stability*, 2013, **1**, 1–75.
[36] G. Ghigliotti, T. Biben and C. Misbah, *Journal of Fluid Mechanics*, 2010, **653**, 489.
[37] A. Lamura and G. Gompper, *EPL (Europhysics Letters)*, 2013, **102**, 28004.
[38] A. Dörr, A. Sadiki and A. Mehdizadeh, *Journal of Rheology*, 2013, **57**, 743–765.
[39] V. Doyeux, S. Priem, L. Jibuti, A. Farutin, M. Ismail and P. Peyla, *Physical Review Fluids*, 2016, **1**, 043301.
[40] J. Zhang, D. Vola and I. A. Frigaard, *J. Fluid Mech.*, 2006, **566**, 389–419.
[41] N. J. Balmforth and A. C. Rust, *J. Non-Newtonian Fluid Mech.*, 2009, **158**, 36 – 45.
[42] A. Vikhansky, *Phys. Fluids*, 2009, **21**,.
[43] A. Vikhansky, *J. Non-Newtonian Fluid Mech.*, 2010, **165**, 1713 – 1716.
[44] B. Albaalbaki and R. E. Khayat, *J. Fluid Mech.*, 2011, **668**, 500–550.
[45] O. Turan, N. Chakraborty and R. J. Poole, *J. Non-Newtonian Fluid Mech.*, 2012, **171-172**, 83 – 96.
[46] A. Davaille, B. Gueslin, A. Massmeyer and E. Di Giuseppe, *Journal of Non-Newtonian Fluid Mechanics*, 2013, **193**, 144–153.
[47] A. Massmeyer, E. Di Giuseppe, A. Davaille, T. Rolf and P. J. Tackley, *Journal of Non-Newtonian Fluid Mechanics*, 2013, **195**, 32–45.
[48] Z. Kebiche, C. Castelain and T. Burghelea, *Journal of Non-Newtonian Fluid Mechanics*, 2014, **203**, 9–23.
[49] N. J. Balmforth, I. A. Frigaard and G. Ovarlez, *Annu. Rev. Fluid Mech.*, 2014, **46**, 121–146.
[50] M. Hassan, M. Pathak and M. K. Khan, *J. Non-Newtonian Fluid Mech.*, 2015, **226**, 32 – 45.
[51] I. Karimfazli, I. Frigaard and A. Wachs, *Journal of Fluid Mechanics*, 2016, **787**, 474–507.
[52] H. Bénard, *Rev. Gen. Sci. Pures Appl.*, 1900, **11**, 1261–1271.
[53] L. Rayleigh, *The London, Edinburgh, and Dublin Philosophical Magazine and Journal of Science*, 1916, **32**, 529–546.

[54] G. Ahlers, S. Grossmann and D. Lohse, *Reviews of modern physics*, 2009, **81**, 503.

[55] F. H. Busse, *Rep. Prog. Phys.*, 1978, **41**, 1929–1967.

[56] D. Lohse and K.-Q. Xia, *Annual Review of Fluid Mechanics*, 2010, **42**, 335–364.

[57] F. Chillà and J. Schumacher, *The European Physical Journal E*, 2012, **35**, 1–25.

[58] S. Succi, *The lattice Boltzmann Equation*, Oxford University Press, 2018.

[59] T. Krüger, H. Kusumaatmaja, A. Kuzmin, O. Shardt, G. Silva and E. M. Viggen, *Springer International Publishing*, 2017, **10**, 4–15.

[60] R. Benzi, M. Sbragaglia, S. Succi, M. Bernaschi and S. Chibbaro, *J. Chem. Phys.*, 2009, **131**,.

[61] P. Ripesi, L. Biferale, M. Sbragaglia and A. Wirth, *Journal of fluid mechanics*, 2014, **742**, 636–663.

[62] R. Benzi, M. Sbragaglia, P. Perlekar, M. Bernaschi, S. Succi and F. Toschi, *Soft Matter*, 2014, **10**, 4615–4624.

[63] B. Dollet, A. Scagliarini and M. Sbragaglia, *J. Fluid Mech.*, 2015, **766**, 556–589.

[64] F. Pelusi, M. Sbragaglia and R. Benzi, *Soft matter*, 2019, **15**, 4518–4524.

[65] G. Falcucci, G. Bella, G. Chiatti, S. Chibbaro, M. Sbragaglia, S. Succi *et al.*, *Communications in computational physics*, 2007, **2**, 1071–1084.

[66] R. Benzi, M. Bernaschi, M. Sbragaglia and S. Succi, *Europhys. Lett.*, 2010, **91**, 14003.

[67] R. Benzi, M. Sbragaglia, A. Scagliarini, P. Perlekar, M. Bernaschi, S. Succi and F. Toschi, *Soft Matter*, 2015, **11**, 1271–1280.

[68] X. Shan, *Physical Review E*, 2008, **77**, 066702.

[69] M. Sbragaglia and D. Belardinelli, *Physical Review E*, 2013, **88**, 013306.

[70] M. Bernaschi, L. Rossi, R. Benzi, M. Sbragaglia and S. Succi, *Phys. Rev. E*, 2009, **80**, 066707.

[71] A. Scagliarini, M. Sbragaglia and M. Bernaschi, *J. Stat. Phys.*, 2015, **161**, 1482–1495.

[72] F. Pelusi, M. Sbragaglia, A. Scagliarini, M. Lulli, M. Bernaschi and S. Succi, *EPL (Europhysics Letters)*, 2019, **127**, 34005.

[73] D. J. Jeffrey and A. Acrivos, *AIChE Journal*, 1976, **22**, 417–432.

[74] R. G. Larson, *The Structure and Rheology of Complex Fluids*, Oxford University Press, 1999.

[75] A. Einstein, *Annalen der physik*, 1906, **324**, 371–381.

[76] B. I. Shraiman and E. D. Siggia, *Physical Review A*, 1990, **42**, 3650.

[77] R. J. Stevens, R. Verzicco and D. Lohse, *Journal of Fluid Mechanics*, 2010, **643**, 495–507.

[78] F. Pelusi, M. Sbragaglia, R. Benzi, A. Scagliarini, M. Bernaschi and S. Succi, *Convective heat transfer of a model emulsion at the droplet scale*, http://arxiv.org/abs/2010.02139, 2020.

[79] R. Benzi, E. S. Ching, C. Wilson and Y. Wang, *Journal of Fluid Mechanics*, 2016, **788**, 337–357.

[80] S. D. Hudson, *Physics of fluids*, 2003, **15**, 1106–1113.

[81] N. O. Jaensson, C. Mitrias, M. A. Hulsen and P. D. Anderson, *Langmuir*, 2018, **34**, 1795–1806.

[82] A. R. Malipeddi and K. Sarkar, *Physical Review Fluids*, 2019, **4**, 093603.